International Conference on Space Optics—ICSO 2022

Dubrovnik, Croatia

3–7 October 2022

Edited by Kyriaki Minoglou, Nikos Karafolas, and Bruno Cugny,

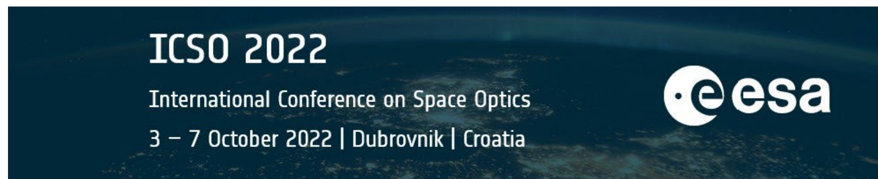

Spatially resolved scattering metrology to quantify losses induced by contamination and defects

International Conference on Space Optics — ICSO 2022, edited by Kyriaki Minoglou, Nikos Karafolas,
Bruno Cugny, Proc. of SPIE Vol. 12777, 127776I · © 2023 ESA and CNES · 0277-786X · doi: 10.1117/12.2691131

Spatially resolved scattering metrology to quantify losses induced by contamination and defects

Bolliand A.[a], Zerrad M.[a], Lequime M.[a], and Amra C.[a]

[a]Aix-Marseille Université, Ecole Centrale Marseille, CNRS - Institut Fresnel, UMR 7249

ABSTRACT

In less than 20 years, extraordinary progress has been made on the design and manufacturing of planar optical components, especially in terms of minimizing light scattering (a few 10^{-6} of the incident flux). This progress is closely linked to polishing techniques, which allow to obtain, on amorphous substrates, roughness lower than a fraction of nanometer in the optical frequency window. Moreover, with modern filter manufacturing technologies, the roughness of the substrate is reproduced almost identically by each of the thin layers constituting the stack.

However, at this level of qualification, new problems and concerns arise, in particular the presence of localized defects in the component. These defects are of sub-micron size and appear during the manufacturing of the filters. Their density is low (less than one defect for a 100 micrometers diameter disk), so for conventional components, their contribution can be neglected. However, for Space optics and gravitational waves detection, the impact of these isolated defects can become dominant in the light scattering process and its accurate quantification remains a challenge.

To address this problematic, the CONCEPT Group of the Institut Fresnel developed a SPatially and Angulary Resolved Scatterometry Equipment (SPARSE). The principle of the instrument is based on the coupling of imaging abilities with a scatterometer. It is designed to record up to 440 thousand BRDF with a single measurement on a one inch diameter component. A beam shaping arm is added to tailor the illumination to the shape of the component and to offer the capability to “turn off” defects in order to increase the detectivity. SPARSE allows the measurement of scattering level as low as $10^{-8} sr^{-1}$ and the data processing is designed to discriminate and quantify the weight of localized defects, contamination, scratches and roughness in the scattering budget.

We propose in this paper a detailed description of the set-up with its metrological qualification and some examples of measurements performed on representative Space Optics.

Keywords: scattering, defects, contamination, thin-films, Surface analysis, roughness

1. INTRODUCTION

1.1 Context

Parasitic light scattered by optical components is one of the main limitations of the performances of extrem optical systems such as optical payloads for Earth and Space observation or interferometer for Gravitationnal Waves detection. The scattered light can originate from different sources intrinsec to the manufacturing, such as surface roughness, optical coatings or bulk inhomogenehities, but also from the presence of defects and contaminants. In this context, the last few years have seen new challenges merge on the metrology and control of scattering losses.

More precisely, while manufacturing techniques improves, scattered light from defects and contaminants is more and more predominant in scattering budgets. In this paper we will present a new SPatially and Angulary Resolved Scatterometry Equipment (SPARSE), that will address this problematic by discriminating and quantifying the light scattered by the manufactured intrinsic roughness and the light scattered by unwanted defect or contaminant.

Further author information:
Send correspondence to: Bolliand A., E-mail: adrien.bolliand@fresnel.fr, Telephone: +33 6 72 20 52 39

1.2 Theoretical background for scattered light

Here we will quickly describe what the instrument will measure from the electromagnetic theory. If we constrain ourselves too smooth surfaces, we can use the 1st order theory to describe the power spectral density of the scattered light: $J(\sigma_x, \sigma_y)$ with (σ_x, σ_y) the spatial pulsation.[1–4]

$$J(\sigma_x, \sigma_y) = C(\sigma_x, \sigma_y) \cdot \gamma(\sigma_x, \sigma_y) \cdot \Phi_0 \tag{1}$$

$C(\sigma_x, \sigma_y)$ is a term linked to the properties of a specific surface, it derives from electromagnetic theory. Φ_0 is the power of the incident light source and $\gamma(\sigma_x, \sigma_y)$ is the roughness spectrum of the surface. We define the angles (θ_i, θ_s). θ_i is the angle between the normal to the scattering surface and the incident light while θ_s is the angle between the normal to the scattering surface and a scattered direction. As we will see later, with the instrument described in this paper, the detection angle is constant, and fixed at 0°. Therefore, we can now consider that $\theta_s = 0°$, and considering the power spectral density we can define the intensity of the light scattered from an incident angle θ_i:

$$I(\theta_i) = \left(\frac{2\pi n_0}{\lambda}\right)^2 J(\sigma, 0) \cdot cos(\theta_i) \tag{2}$$

And with a scatterometer, we measure, for a solid angle, the ratio of the intensity of the light scattered by a surface with the optical power of the incident beam. In our case, for this paper we will only look at reflected scattered light so the cosine corrected BRDF as defined by Nicodemus[5] or the $ARS(\theta_i)$ for the scattering angles $(\theta_i, \theta_s = 0)$.

$$ARS(\theta_i) = BRDF \cdot cos(\theta_i) = \frac{I(\theta_i)}{\Phi_0} \tag{3}$$

1.3 Principle of scatterometer apparatus

The scatterometer that we will describe in the paper deviate from the usual way to measure scattered light. It may be useful to describe, in principle, how scatterometers usually work and to explain how SPARSE is different.

See Fig. 1, on the left is the principle of classical scatterometer. It is usually a fixed light source illuminating a sample (so θ_i is constant), and a detector − usually a photodiode − rotating around the sample, measuring scattered light (so it scans θ_s). This is great for a lot of applications, but since we want to be able to differentiate the light scattered by the intrinsic roughness out of the light scattered by defects, we cannot use a photodiode that will average the light scattered from an area of the sample.

Instead, we would like to use a CCD to image the sample, but in order to keep a constant mapping between surface element of the sample and a pixel of the CCD, we need to keep the detection angle, θ_s, constant. And instead have the illumination angle to rotate. We can see this configuration in the middle of Fig. 1. It is also the configuration of AOS described in [6].

SPARSE configuration is similar on the principle. But we wanted to add the functionality of adapting the illumination to potential defects on the sample that would blind the instrument. This made the illumination source larger, heavier and difficult to rotate around a sample. So instead, the sample is physically linked to the CCD camera and both are rotating around a fixed light source on the optical table. Therefore, in the sample reference it is indeed the source that is rotating and the instrument is scanning θ_i. In Fig. 2, we can see a schematic of the instrument that is described in the next section.

2. INSTRUMENT DESCRIPTION

2.1 Overview

SPARSE purpose is to perform $ARS(\theta_i)$ measurements with high sensitivity, down to $10^{-8} sr^{-1}$. The instrument is automated, it measures scattered light scanning the incident angle θ_i the measurement angle θ_s is fixed at 0°. The next subsections will describe some of the key elements of SPARSE.

SPARSE is built upon the heritage of AOS (Optical Surface Analyzer) described in [6]. It is the assembly of:

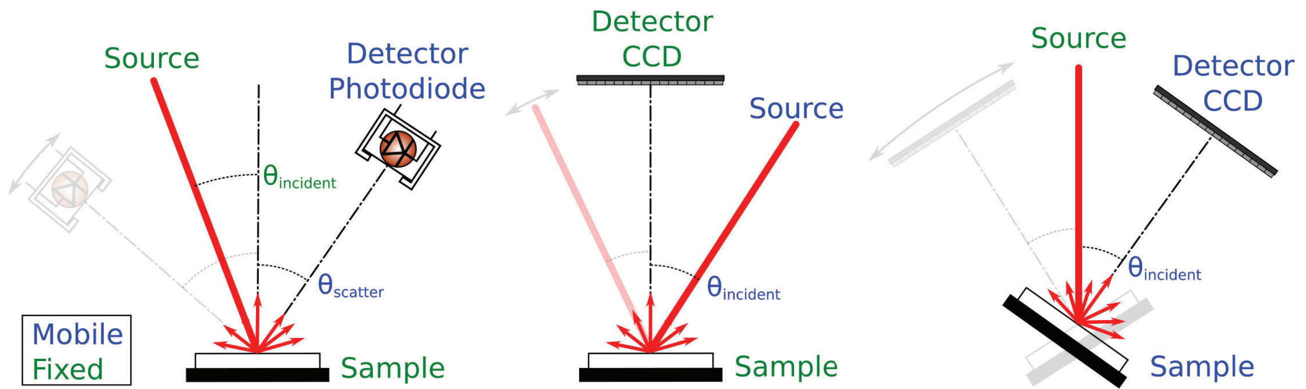

Figure 1. Scatterometer principle. On the left, a classical scatterometer set up. in the middle, the AOS set up, on the right SPARSE set up.

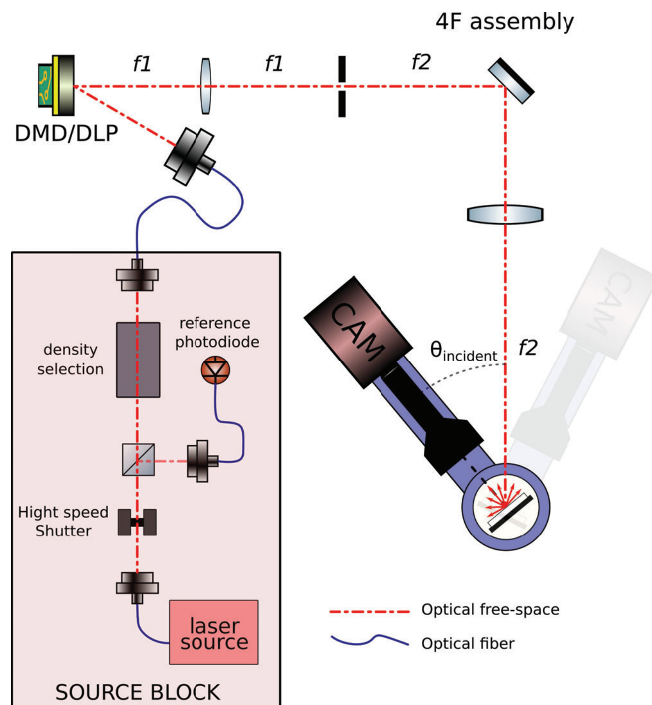

Figure 2. Schematic of SPARSE assembly.

- A source block, controlling the intensity of the main illumination beam and the exposure time.
- An imaging system, combining a highly sensitive CCD camera with a telecentric lens, both mounted on a rotary stage with a sample to analyze.
- An adaptive illumination system combining a Digital Micro-mirror Device (DMD) and a 4F assembly. It can project any illumination pattern we need on the sample.

2.2 Source block

The source is a red laser diode (SLD635B) centered at 635 nm ($\pm 6\ nm\ at\ 3dB$). The bandwidth of the spectrum cancel some of the speckle from the coherent laser, while being similar to a monochromatic configuration. With the source block, we can control the intensity of the light beam with a set of optical densities and the exposure time with a high-speed shutter. This shutter is used to command a precise and repeatable exposure time, which

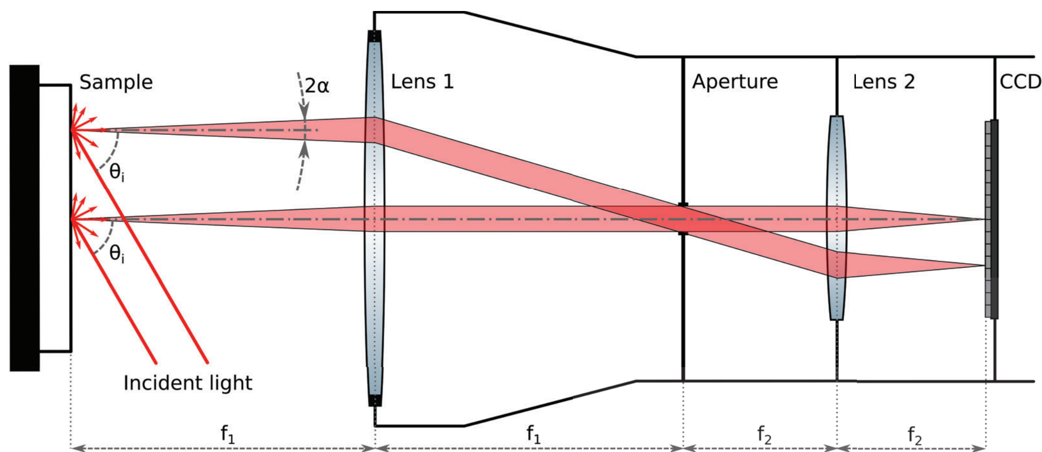

Figure 3. Showing how the scattered light is being measured with a telecentric lens. θ_i is the incident angle of the source light. α is the half-divergence of the scattered beam collected on the CCD.

is more reliable than the camera built in shutter. During the measurement, the output power of the diode laser is recorded with the reference photodiode, this enables us to consider potential power fluctuation of the source.

2.3 Imaging system

The camera is a PIXIS 1024B with a CCD array of 1024×1024 pixels, back illuminated, with a 100% fill factor. The pixels are square and 13 μm wide. The dark current is limited to $0.001 e^{-} pixel^{-1} s^{-1}$ thanks to a thermoelectric cooler regulating the camera sensors at $-70°C$.

A telecentric lens is mounted on the camera. The telecentric lens is critical for this application. With it, the camera "sees" the sample without any distortion due to a field of view. This guarantee that, for every point on the sample, we are measuring light scattered in the direction of all parallels chief rays, perpendicular to the CCD with a half-divergence angle α. The half-divergence of the scattered beam collected by the system is $\alpha = arctan(\frac{G}{2N})$. With a magnification G set at 0.5, and the aperture number N selected at 10.2, the half-divergence α is around $1.4°$. The principle of the measurement with the telecentric lens if shown Fig. 3.

2.4 Adaptive illumination

Since defects or contaminants scatter more than the intrinsic roughness of a sample, a defect can "blind" the sensor. Because we would lose information on saturated pixels, the instrument operations are designed to avoid it. It is like tying to look at deemed stars next to the moon. But unlike in astronomy we cannot occult a defect. So instead we will remove the beam of light illuminating it. Thanks to the use of a Digital Micro-mirror Device (DMD), we are capable to adapt the illumination to every sample, it is one of the unique features of SPARSE compared to other scatterometer.

Briefly, a DMD is an array of mirrors that we can set the position into one of two stable orientations. Every mirror of the 1024×768 array can be controlled to shine light in the direction of the optical axis – to the sample being analyzed – or to shine light into a light dump. A DMD, coupled with a 4F assembly (see Fig. 2) enable us to illuminate the sample with any shape we want – as long as the resolution of the DMD allows it.

We can control the DMD by sending it a black and white image of 1024×768 pixels. A white pixel will illuminate the sample, a black pixel will block the light. And since we are changing the illumination angle (θ_i) we need to adapt the illumination so that the illumination patters stays constant on the sample at every θ_i.

To do so, we can look at the transformation that an illumination pattern is going through the instrument. Indeed, with our CCD camera, we are looking at an image of the DMD array on the sample. We can see the DMD array and the CCD array as two vector spaces with an affine transformation between them. If we can describe this affine transformation, it would enable us to project on the sample any illumination we need. By using the SPARSE set-up itself, this affine transformation can be determined from measurements. By installing a white

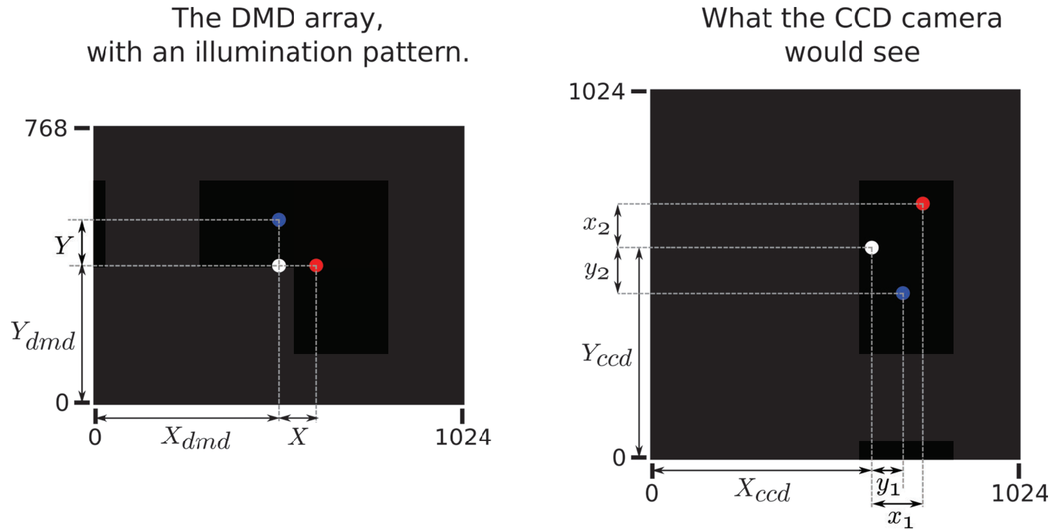

Figure 4. Showing the important parameters to describe the linear transformation between the DMD array to the CCD array.

lambertian sample, we can clearly see the image of the DMD array on the sample and measure the parameters of the linear transformation.

To describe the affine transformation, we need two matrices:

- A linear transformation matrix A (2×2).
- An offset matrix B (2×1).

$$A = \begin{bmatrix} \frac{x_1}{X} & \frac{y_1}{Y} \\ \frac{x_2}{X} & \frac{y_2}{Y} \end{bmatrix} \tag{4}$$

$$B = \begin{pmatrix} X_{ccd} \\ Y_{ccd} \end{pmatrix} - A \cdot \begin{pmatrix} X_{dmd} \\ Y_{dmd} \end{pmatrix} \tag{5}$$

Now, for a pattern on the DMD, we can predict what will be projected on the CCD. For every point of the DMD (x_{dmd}, y_{dmd}) it will shine on the CCD at the position:

$$\begin{pmatrix} x_{ccd} \\ y_{ccd} \end{pmatrix} = A \cdot \begin{pmatrix} x_{dmd} \\ y_{dmd} \end{pmatrix} + B \tag{6}$$

But it is more convenient to be able to command the DMD for a certain shape. This is what we need to do if for example we would need to turn off a defect. We would need to command the DMD to turn off some pixels. Therefore we need to know the inverse transformation. And since the transformation is affine, it can be easily determined. A pixel at the position (x_{ccd}, y_{ccd}) is illuminated by a pixel on the DMD at the position (x_{dmd}, y_{dmd}):

$$A^{-1} \cdot \begin{pmatrix} x_{ccd} \\ y_{ccd} \end{pmatrix} + A^{-1} \cdot B = \begin{pmatrix} x_{dmd} \\ y_{dmd} \end{pmatrix} \tag{7}$$

We can use this to command the DMD for any illumination we need. An example can be seen on Fig. 5, the image on the left shows the illumination that we want projected on the sample and on the right, the transformed image that we need to give to the DMD for $\theta_i = 20°$. This illumination pattern corresponds the max illumination patterns that we can project on a one inch sample. The max illumination pattern covers as much as possible a 1-inch sample, avoiding the edges and the sample holder, hence its shell-like shape (see Fig. 6).

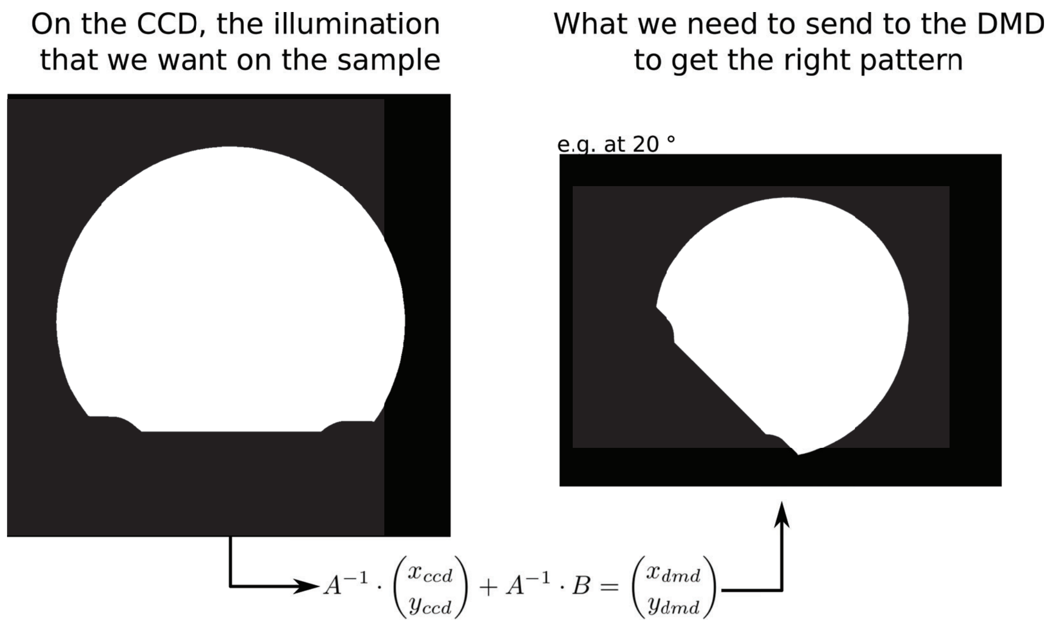

Figure 5. Example of transformation for $\theta_i = 20°$. The image transformation is executed with the warpAffine function of the cv2 library using the interpolation flag: INTER_NEAREST_EXACT to avoid gray pixels (OpenCV external link).

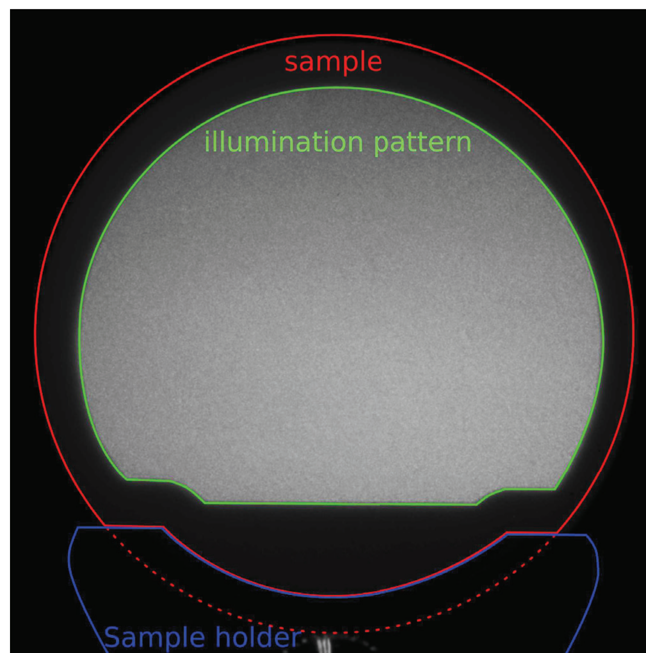

Figure 6. Showing an image (1024) taken with SPARSE's camera. The edges of the different elements are highlighted: the sample holder in blue, the 1 inch sample in red and the max fill illumination pattern projected on the sample in green. The sample is the white lambertian used for the calibration of the instrument.

2.5 Data treatment

The CCD array used for an image acquisition can be seen as an array of light wells. For every pixel (x, y) of the CCD array, we can record a number up to 2^{16}, representative of the number of photons hitting each pixel during the exposure time.

If a value of a pixel $P_{ixelvalue}(x, y)$, is above 40 (out of 2^{16}) the value is considered to be worthy of interpretation. With it we can compute for every pixel (x, y) a "treated value": T_d.

$$T_d(x, y) = C_{acqui} \cdot P_{ixelvalue}(x, y) \tag{8}$$

With C_{acqui} being a coefficient made to compensate the acquisition parameters. This coefficient enables to have comparable data for every exposure time, optical density or laser power fluctuations. The coefficient is the same for all pixels (x, y) of an image but is different for every acquisition. To compute C_{acqui}, the light source intensity is recorded during the acquisition with a photodiode. The sample rate is set to $10^5\ Hz$. This signal is integrated over the time into one number E_{diode}. And with, t_{OD}, the overall transmittance of the density selection devices (see Fig. 2), we computed the coefficient C_{acqui}:

$$C_{acqui} = \frac{1}{t_{OD} \cdot E_{diode}} \tag{9}$$

Then to convert this information into $ARS(\theta_i)$ we still need to calibrate the instrument. This process is described in the next section. During the calibration process, we will find a matrix: $C_{cali}(x, y)$ that will be different for every pixel to compensate the input light uniformity. With this information for every pixel (x, y) we can compute the $ARS(\theta_i)$:

$$ARS(\theta_i)(x, y) = C_{cali}(x, y) \cdot T_d(x, y) \tag{10}$$

3. FIRST MEASUREMENTS

3.1 Instrument calibration with lambertian diffuser

In the previous section, 2.5 we saw that we can output "treated data" T_d out of the instrument. This value is a relative value that can be compared to other measurements of the instrument. But if we want to convert this information into $ARS(\theta_i)$ we need to calibrate the instrument. This can be done thanks to a lambertian diffuser. For this purpose we used the 1-inch SC-10089-T0A sample from Labsphere with an albedo $\rho = 0.98$. The theoretical response of the perfect diffuser is:

$$R_{diffuser}(\theta_i) = A \cdot cos(\theta_i + \delta) \tag{11}$$

Where A is the normalization parameter that we can determine for every illuminated pixel by the least square method. δ is the offset angle between the knowledge of the illumination angle and the true illumination angle. Knowing A, it is possible to compute C_{cali} which is used to compute $ARS(\theta_i)$ out of treated data.

$$C_{cali}(x, y) = \frac{\rho}{\pi \cdot A} \tag{12}$$

For this measurement, we positioned the sample into its holder and acquired images at angles between 15° and 90°. The max illumination pattern is used.

For every illuminated pixel, we can plot the response of the white lambertian as "treated data". Since the response of the calibrated diffuser is known, we can find the normalization parameter A by a least square method and the offset angle δ between the input position θ_i and its true position. The offset δ was not found by the least square method but by looking at the extinction of the sample that should happen at $\theta_i = 90°$. The extinction is particularly visible on the log scale, it has been found at 0.6° (see bottom plot Fig. 7). Since this angle is simply an offset between the true incident illumination and our knowledge of it, has been ignored in the rest of this article. Once δ is set, the least square method was applied on the response of every illuminated pixel in order to find the value of A. An example, for the pixel (510,510), can be seen on Fig. 7. The Fig. 8 shows on the left

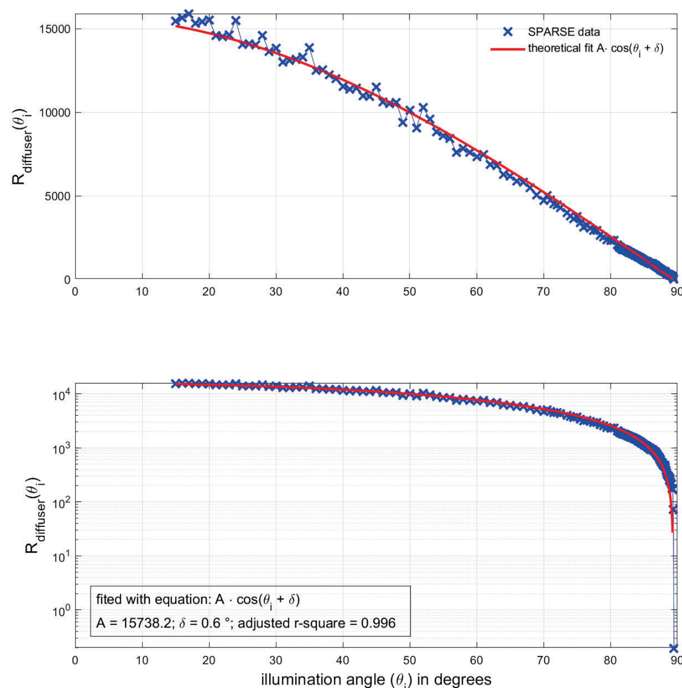

Figure 7. Comparing theoretical fit (red) and acquisition data (blue) of the single pixel: (510,510). The log plot on the bottom allows to clearly assess the offset angle δ thanks to the sharp extinction for $\theta_i + \delta = 90°$. The top plot on a linear scale let us visually assess the fit of the normalizing parameter A.

a plot of all the A values found for every illuminated pixel. On the right a map of the adjusted r-square value, which gives an appreciation of the quality of the fit. It can be noted that on the left of the illuminated pattern the agreement decrease. In sec. 3 we will see that with an other sample, measurements artifacts appears in those regions too. This suggests that there might be an issue with the telecentric objective.

Overall, the calibration was successful which allows us to quantify the $ARS(\theta_i)$ of any other samples. In the next section, we analyzed a silver coated mirror to demonstrate some of the capabilities of the instrument.

3.2 Measurement on a silver coated mirror

We placed in the sample holder a protected silver coated mirror PF10-03-P01 1-inch (thorlabs external link). We first used the max illumination pattern, and in the same condition than during the calibration we took images for every angle between 15° and 89°. The overall quality of the mirror is good, it is silver coated, so we can expect low $ARS(\theta_i)$ over most of the sample surface while seeing scattering hot spots. The manufacturer declares that there could be scratches and dig on the surface. Moreover the instrument is not yet in a clean room, therefore it can be expected to find highly scattering contaminants on the surface. The illuminated surfaced counts 439813 pixels. It is not relevant to display the $ARS(\theta_i)$ of every pixel. Instead we can have an overall look at the sample by computing the Total Integrated Scattering (TIS) map.

$$TIS(x,y) = 2\pi \int_{\theta_i} ARS(\theta_i)(x,y) \cdot sin(\theta_i) d\theta_i \tag{13}$$

For every picture, the exposure time is selected to use as much as possible the 2^{16} value range of the camera. Therefore the exposure time is maximized so that the pixel receiving the most photon does not saturate. Since defects and contaminants scatters light by orders of magnitude more, the range of the camera is not enough and

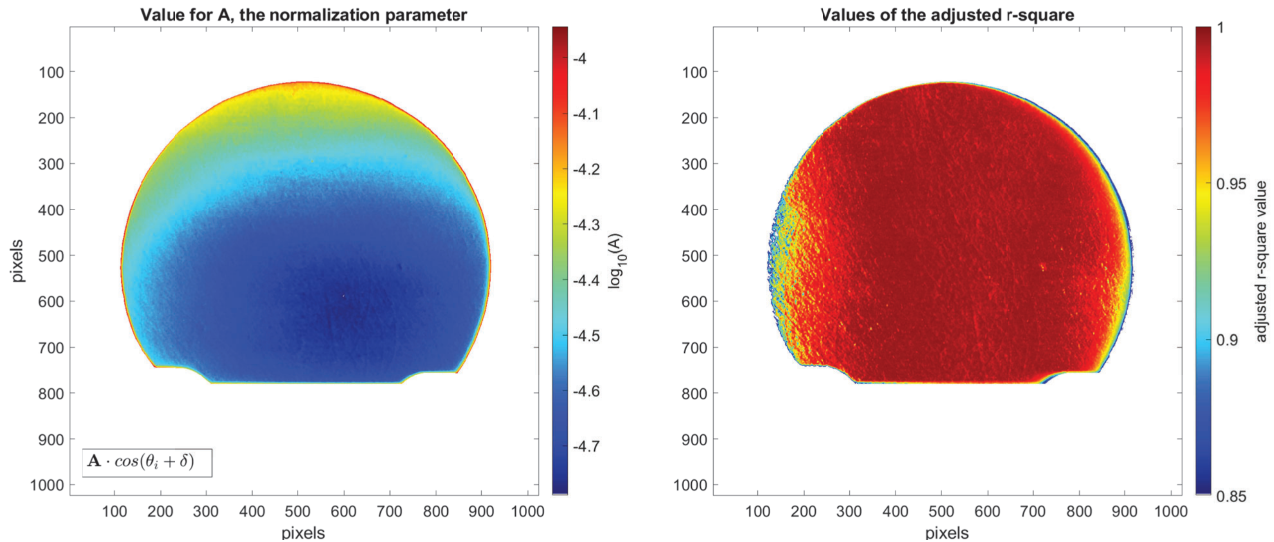

Figure 8. The result of the calibration process. The maps are showing the results for the pixel that have been illuminated. On the left, is a map of the log value of A: the normalization parameter found for each illuminated pixel. The plot on the right is showing a map of the adjusted r-square value of the least square method applied to find A, suggesting good agreement for most illuminated pixels.

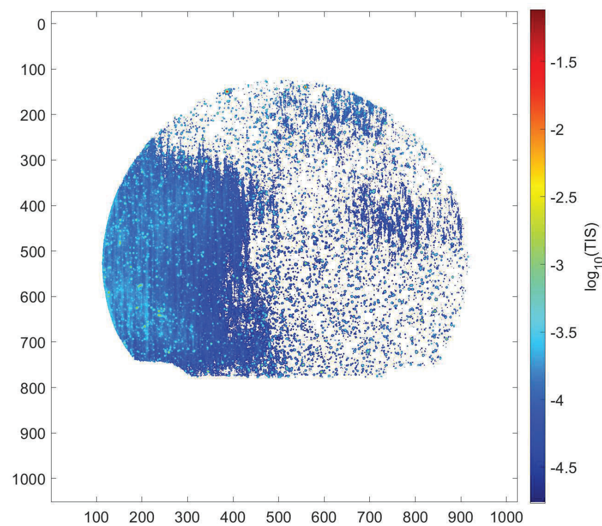

Figure 9. TIS map of the 1 inch silver deposited mirror, acquired with the max illumination pattern.

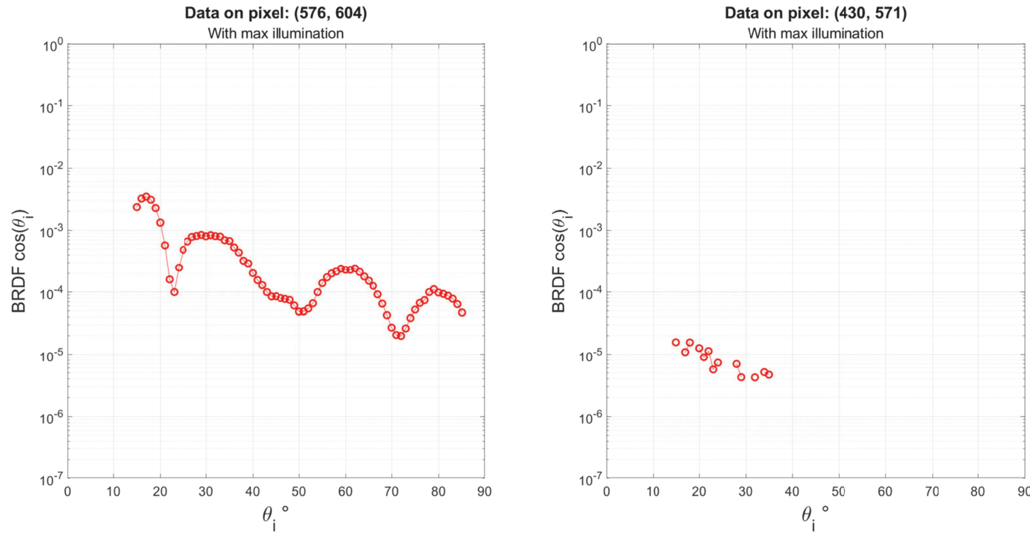

Figure 10. Showing the $BRDFcos(\theta_i)$ measurements on two pixels isolated pixel.

the smoothest part of the mirror do not emit enough photon for the camera to collect meaningful signal, fewer than 40 counts out of 65536 (2^{16}). So for an angle θ_i, if a pixel did not receive enough light, the information is rejected. And if, for a pixel, more than half of the ARS points were rejected, the TIS is also considered as invalid. Hence why most of the pixel, within the illumination patter, are white for "no information". The pixels outside the illumination pattern are also not considered and are colored in white. On the left of the sample, we can see a region that scatter more than the rest of the mirror. We think it is a measurement artifact, maybe due to a issue with the telecentric objective. The information on this part of the sample is not relevant. This issue will be further investigated and sorted as soon as possible.

When we look at the TIS, since most of the sample did not emit enough photons, the imager mostly studied the defects, but very little information has been gathered about the smooth parts of the surface due to the short exposure time.

We can also observe this by looking at the ARS plot of specific pixels. On the Fig. 10 we see for the pixel (546,604) that the ARS pattern, most likely the one a defect, scattered up to $2 \cdot 10^{-3} sr^{-1}$. The pixel was chosen because it stood out on the TIS map. And indeed it shows an ARS curve characteristic of a defect.
But the pixel (430,571) is most likely imaging a smooth part of the mirror, free from defects, that did not scattered enough light on most incident angles to be correctly interpreted.

To be able to study smooth, low scattering, parts of the sample, we can use the DLP to project an adapted pattern that will remove light from highly scattering defects. If on the TIS map we mark the top 2% scattering pixels and remove them from the illumination pattern, we should be able to increase the exposure time and collect more photons from smooth areas of the sample.

3.3 Measurement on the silver coated mirror with adapted illumination

With the same sample, and in the same condition, we repeated the acquisition but with the new adapted illumination patter. With it, we could scan θ_i between 15° and 71°. Beyond 71°, the integrity of the illumination pattern cannot be guaranty due to the finite resolution of the DMD. The pattern is shown on the bottom right of Fig. 11. For this acquisition, the exposure time of the images drastically increased as it can be seen on Fig 12. The exposure topped at 400 s, the maximum allowed exposure time at the moment, to keep the overall acquisition process within reasonable time. This allows the CCD to collect more photons from the low scattering areas of the sample. And if we look at the new TIS map (Fig. 13) or we look back at pixel (430,571)(Fig. 14), we can see that with the adapted illumination the instrument is capable to get information about low scattering part of the mirror.

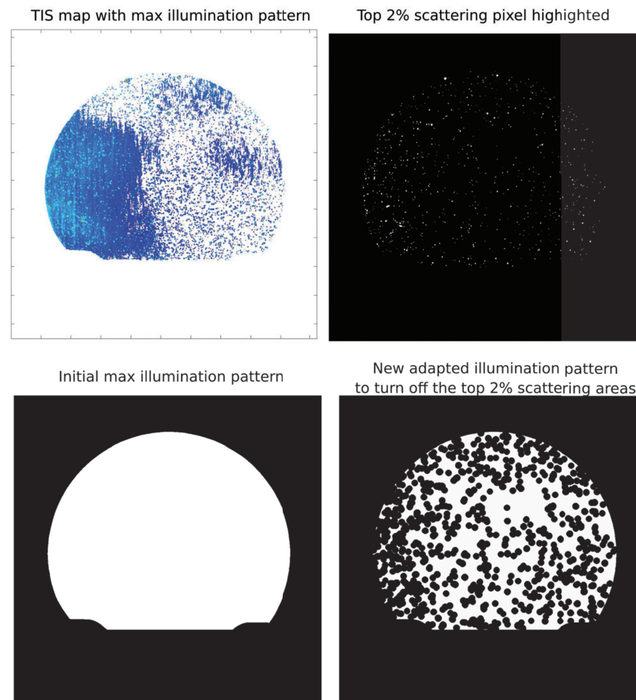

Figure 11. Showing how an adaptive illumination pattern can be made. On the top left, the TIS map of the mirror sample, on the top right, in white, the top 2% scattering pixels. On the bottom left, the original max illumination pattern and on the right, the new illumination pattern with dark spot where top scattering areas where found.

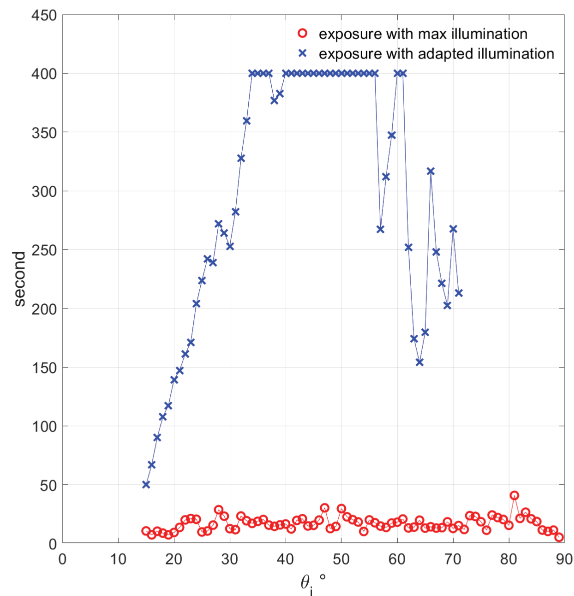

Figure 12. Comparing exposure times for every images take for a certain incident angle θ_i. In red the exposure time for the acquisition with the max illumination pattern and in blue for the acquisition with the adapted illumination pattern. The exposure time with the adapted illumination pattern reached 400 s the maxmimum allowed by the system at the moment.

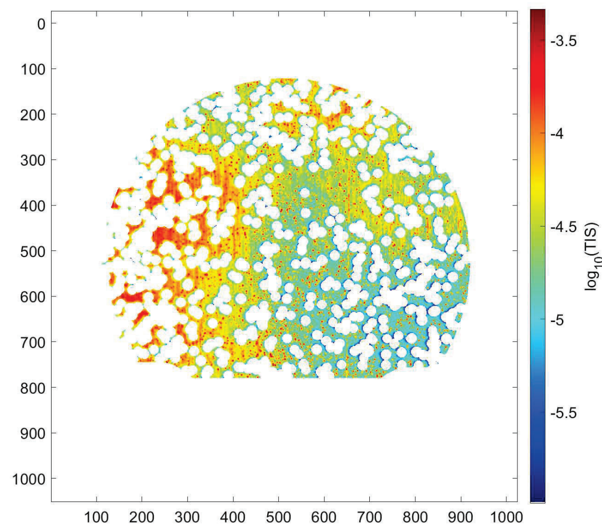

Figure 13. TIS map of the 1 inch silver deposited mirror, acquired using the adapted illumination pattern that obscured highly scattering areas of the sample.

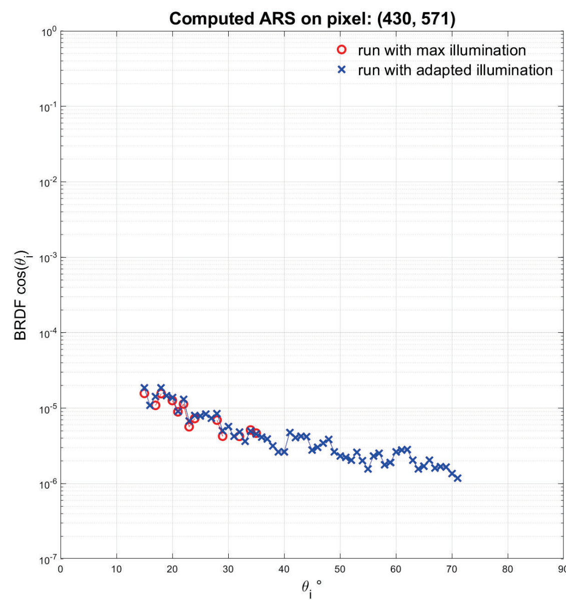

Figure 14. Comparing two sets of ARS measurement on the same pixel but executed with different illumination patterns. In red an acquisition with the max illumination pattern trying to measure ARS between 15° and 89°. In blue the ARS acquisition with the adapted illumination pattern trying to measure ARS between 15° and 71°.

By considering both measurements, one with the max illumination patterns, that gives information mostly about the high scattering areas, and this acquisition, that gives information about the low scattering areas, we will be capable to understand the impact of defects and contaminants on the overall scattering budget.

4. CONCLUSION

This paper described SPARSE, a new scatterometer using imaging capabilities to measure scattered light. SPARSE is capable to measure reflected scattering light, scanning θ_i with from 15° up to 89°, depending on the illumination pattern used. By adapting the illumination pattern with a DMD, we are capable to focus the range of the instrument on collecting light from highly scattering defects or low scattering intrinsic roughness part of the sample.

On the short term by improving the data analysis, this instrument can be used to quantify the impact of a defect in regard of the intrinsic roughness of a sample. It should enable us, for example, to tell if the light scattered by contaminants, accumulating in clean room, have a significant effect on the scattering budget. It can also be used to gain information about the topology of a surface, indeed as we seen in the equations Sec. 1.2, from the ARS, we can ultimately get information about γ the roughness spectrum of the surface.

We will improve the hardware. The 1st action to do is to verify the capability of the instrument to measure scattered light in transmission, the BTDF. It should be just a matter of verification, since the instrument as it is, should be able to do it. After that, SPARSE can be upgraded to perform measurements at multiple wavelengths, not just 633 nm. It would enable us to look at the performance of optics in the condition of there specific application. In the future, it could also be upgraded to study the polarisation of the scattered light.

ACKNOWLEDGMENTS

This work has been achieved thanks to the programme ”Investissement d’avenir - ANR-21-ESRE-0002 - Equipex IDEC” for material and to the support Thales Alenia Space and CEA CESTA.

REFERENCES

[1] Amra, C., Lequime, M., and Zerrad, M., [*Electromagnetic optics of thin-film coating*], Cambridge university press, 1 ed. (2021).

[2] Amra, C., “First-order vector theory of bulk scattering in optical multilayers,” *J. Opt. Soc. Am. A* **10**, 365–374 (Feb 1993).

[3] Amra, C., Grèzes-Besset, C., and Bruel, L., “Comparison of surface and bulk scattering in optical multilayers,” *Appl. Opt.* **32**, 5492–5503 (Oct 1993).

[4] Amra, C., “Light scattering from multilayer optics. i. tools of investigation,” *J. Opt. Soc. Am. A* **11**, 197–210 (Jan 1994).

[5] Nicodemus, F. E., Richmond, J. C., Hsia, J. J., Ginsberg, I. W., and Limperis, T., “Geometrical considerations and nomenclature for reflectance,” Tech. Rep. NBS MONO 160, National Bureau of Standards, Gaithersburg, MD (1977).

[6] Lequime, M., Zerrad, M., Deumié, C., and Amra, C., “A goniometric light scattering instrument with high-resolution imaging,” *Optics Communications* **282**, 1265–1273 (Apr. 2009).